Unique semantic space in the brain of each beholder predicts perceived similarity

Ian Charest[a,1], Rogier A. Kievit[a], Taylor W. Schmitz[a], Diana Deca[b], and Nikolaus Kriegeskorte[a,1]

[a]Medical Research Council Cognition and Brain Sciences Unit, Cambridge CB2 7EF, United Kingdom; and [b]Institute of Neuroscience, Technische Universität München, 80802 Munich, Germany

Edited by Leslie G. Ungerleider, National Institute of Mental Health, Bethesda, MD, and approved August 29, 2014 (received for review February 19, 2014)

The unique way in which each of us perceives the world must arise from our brain representations. If brain imaging could reveal an individual's unique mental representation, it could help us understand the biological substrate of our individual experiential worlds in mental health and disease. However, imaging studies of object vision have focused on commonalities between individuals rather than individual differences and on category averages rather than representations of particular objects. Here we investigate the individually unique component of brain representations of particular objects with functional MRI (fMRI). Subjects were presented with unfamiliar and personally meaningful object images while we measured their brain activity on two separate days. We characterized the representational geometry by the dissimilarity matrix of activity patterns elicited by particular object images. The representational geometry remained stable across scanning days and was unique in each individual in early visual cortex and human inferior temporal cortex (hIT). The hIT representation predicted perceived similarity as reflected in dissimilarity judgments. Importantly, hIT predicted the individually unique component of the judgments when the objects were personally meaningful. Our results suggest that hIT brain representational idiosyncrasies accessible to fMRI are expressed in an individual's perceptual judgments. The unique way each of us perceives the world thus might reflect the individually unique representation in high-level visual areas.

visual perception | object representations | representational similarity analysis | neuroimaging | memory

Everyone's perception of the world is unique. Psychologists and psychotherapists, using methods including questionnaires and free association, have long attempted to peer into an individual's subjective experiential world. The unique aspects of our experience coexist with a shared experiential component. We can all recognize the objects that surround us and name them in a common language. Consistent with this shared component of experience, there is evidence that visual stimuli are processed similarly in the brains of different individuals (1). However, the unique way in which each of us perceives an object also must arise from brain activity. Is there an individually unique component to our brain representations?

Unidimensional aspects of subjective visual percepts, ranging from estimates of object size, color, vividness, and emotional valence, have separately been found to correlate with interindividual variation in both univariate regional-average activation and cortical anatomy (2, 3). However, it remains unclear how a person's multidimensional subjective percept reflects the multivariate brain-activity pattern that represents a particular object.

Functional magnetic resonance imaging (fMRI) studies of object vision have focused largely on commonalities among subjects and category averages across particular stimuli. These studies have revealed regions in human inferior temporal cortex (hIT) that preferentially respond to specific categories (4–9) as well as widely distributed category information (10). More recently, similarity analyses of response patterns to particular stimulus images have revealed exemplar-specific representations (11–14), clustering of response patterns by natural categories (15–17), and reinstatement of neural representations during memory recall (18, 19). These prior studies either tacitly assumed similar representations across individuals or explicitly demonstrated commonalities between individuals and even between species (14, 20–29).

Previous studies have shown that the hIT representation has a semantic component (23) and is reflected in perception at the level of group averages (30). Here we tested the hypothesis that an individual's hIT representation predicts idiosyncrasies in his or her perception of natural objects. Because of hIT's reciprocal connections to the memory regions of the medial temporal lobe (31), we further predicted that personally meaningful objects elicit individually unique mnemonic associations and are more distinctly represented in each individual.

We presented familiar and unfamiliar object images to subjects during fMRI and investigated whether early visual cortex (EVC) and hIT exhibit individually unique representations. We characterized the representational geometry of each region by the dissimilarity matrix of activity patterns elicited by particular object images. This matrix is called the "representational dissimilarity matrix" (RDM) (16). To address whether the detailed representational geometries are reflected in behavior, we tested whether individual idiosyncrasies in similarity judgments can be predicted on the basis of a subject's brain RDM.

Results

We used fMRI to measure brain activity while subjects ($n = 20$) were presented with 72 pictures of bodies, faces, places, and man-made objects. We asked our subjects to provide photos that depict personally meaningful objects present in their daily environment (e.g., a parent's face, the front of the subject's own

Significance

Everyone is different. Understanding the unique way an individual perceives the world is a fundamental goal of psychology and brain science. Using novel methods for analyzing functional MRI (fMRI) data, we show that each person viewing a set of objects represents the objects uniquely in his or her brain. Moreover, given an individual's measured brain-activity patterns, idiosyncrasies in his or her perception of the similarities among the objects can be predicted. Prediction accuracy is modest using current technology. However, our results demonstrate that fMRI has the power to reveal individually unique representations of particular objects in the human brain. The novel method might help us understand the biological substrate of individual experience in mental health and disease.

Author contributions: I.C. and N.K. designed the research; I.C. and D.D. performed the experiments; I.C., R.A.K., T.W.S., and N.K. contributed analytic tools; I.C. and N.K. analyzed data; and I.C. and N.K. wrote the paper.

The authors declare no conflict of interest.

This article is a PNAS Direct Submission.

Freely available online through the PNAS open access option.

[1]To whom correspondence may be addressed. Email: ian.charest@mrc-cbu.cam.ac.uk or nikolaus.kriegeskorte@mrc-cbu.cam.ac.uk.

This article contains supporting information online at www.pnas.org/lookup/suppl/doi:10.1073/pnas.1402594111/-/DCSupplemental.

house, or the subject's own vehicle (*Materials and Methods*, Fig. 1*A*, and Fig. S1). Each subject viewed 18 images from his or her own environment (the subject's own "photo album") and 18 images from another randomly assigned subject's environment (that subject's photo album). This subject-pairing strategy enabled us to investigate the effects of object familiarity in the absence of stimulus confounds. All subjects were additionally presented with a standard set of 36 images that were not personally meaningful. Each subject performed similarity judgments on the full set of 72 images (32, 33). The subject then was scanned while viewing the images (day 1). One to two weeks later, the subject was scanned again while viewing the images (day 2).

The regions of interest (ROIs) were defined by anatomical and functional criteria (*SI Materials and Methods*). Briefly, we defined V1, V2, the lateral occipital complex (LOC), the fusiform face area (FFA), and the parahippocampal place area (PPA) for each subject and scanning day. To investigate the distributed representations in EVC and hIT, we additionally defined more inclusive bilateral ROIs. EVC and hIT were each defined by selecting the 1,200 most visually responsive voxels within an anatomical mask. The EVC mask included V1, V2, and V3. The hIT mask spanned a wide expanse of posterior and anterior temporal cortex, including the category-selective regions LOC, FFA, and PPA. The ROIs were defined separately for each subject and scanning day, based on independent anatomical and functional data acquired on that day.

For each ROI, we estimated the activity pattern associated with each particular image, which formed the input to representational similarity analysis (RSA) (16, 34, 35). We computed the representational dissimilarity for each pair of objects as 1 minus the Pearson correlation across voxels. These dissimilarities were assembled in an RDM (a symmetric matrix about a diagonal of zeros).

Consistent with previous studies (23), the hIT activity patterns clustered according to categories (bodies, faces, places, and objects), with smaller representational dissimilarities among objects of the same category. The major categorical division was between animate and inanimate objects (see Fig. 2 *B* and *C* for the group-average RDM in hIT and Fig. 3 for single-subject examples).

Representational Geometries Are Replicable Across Scanning Days. A basic requirement for an investigation of individual differences is that the measurements be reliable within subjects. To assess the replicability of the RDMs between different days of measurement, we compared RDM estimates between scanning days 1 and 2 (Fig. 3) using the Pearson correlation. We constructed a subject similarity matrix, which compares each subject's day 1 RDM with each subject's day 2 RDM. The diagonal entries indicate the within-subject correlations of the RDMs between day 1 and day 2. The off-diagonal entries indicate the between-subject correlations of the RDMs, also between day 1 and day 2. We tested for within- and between-subject RDM replicability using a stimulus-label randomization test (*Materials and Methods* and *SI Materials and Methods*).

We first describe the results for the set of unfamiliar images presented to all subjects. The full set of replicability results is detailed in Figs. S3 and S4. Within subjects, we found replicable representational geometries across scanning days (EVC: $r = 0.32$, $P < 0.0001$; hIT: $r = 0.42$, $P < 0.0001$). Between subjects, both EVC and hIT also have correlated RDMs (EVC: $r = 0.23$, $P < 0.0001$; hIT: $r = 0.32$, $P < 0.0001$). This result reflects the expected similarity of the object representational geometry between subjects, including the conventional categorical divisions that have been reported previously (4–17).

For personally meaningful objects, we also observed replicable representational geometries within and between subjects. Within-subject replicabilities were significant for both regions (EVC: $r = 0.20$, $P < 0.0001$; hIT: $r = 0.40$, $P < 0.0001$). The analysis of between-subject replicabilities for the personally meaningful objects was constrained to paired subjects who had viewed identical image sets (their own and each other's photo albums; *SI Materials and Methods*). Between subjects, as well, both EVC and hIT had correlated RDMs (EVC: $r = 0.17$, $P < 0.0001$; hIT: $r = 0.30$, $P < 0.0001$). In sum, representational geometries were clearly replicable in both EVC and hIT for unfamiliar and familiar objects and within and between subjects.

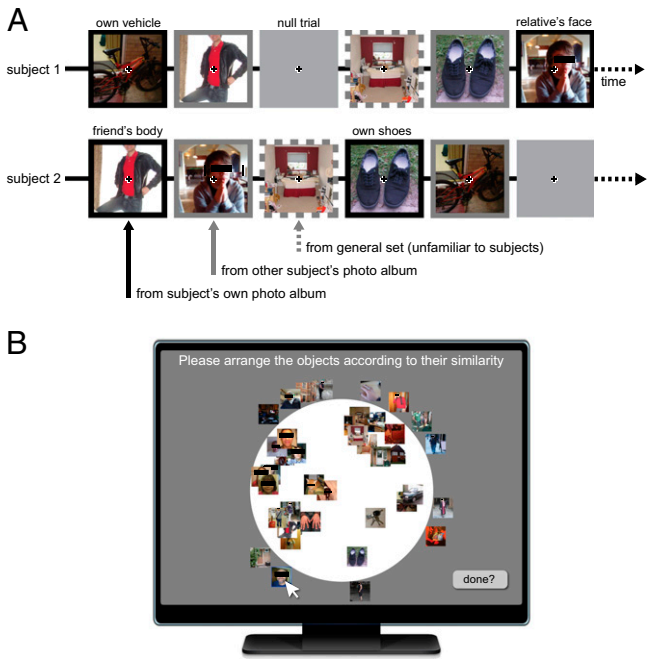

Fig. 1. Experimental design. (*A*) Brain-activity measurement. Subjects were grouped in pairs who viewed their own and each other's personally meaningful object images. There were 10 pairs of subjects. Each subject viewed a total of 72 images in an event-related fMRI experiment, enabling us to estimate the response pattern for each particular image. Among the 72 images, 18 were from the subject's own photo album, and 18 were from the paired subject's photo album. The remaining 36 images were unfamiliar images viewed by all subjects. For the full set of images for one pair of subjects, see Fig. S1. Subjects fixated on a central cross and performed an anomaly detection task. (*B*) Behavioral measurement. Each subject also judged the similarity of the objects by arranging them on a computer screen, so that the distance between any two objects reflected their subjective dissimilarity. In the first trial, the subject arranged all 72 images. On subsequent trials, the subject arranged subsets designed adaptively to estimate optimally the potentially high-dimensional dissimilarity structure (see ref. 33 for details). Eye regions are occluded above in the images to protect privacy, but were not occluded in the experiments.

Representational Geometries Are Individually Unique in EVC and hIT. The analysis described above showed that an individual's representation is replicable across scanning days and that it is similar to the representation in other individuals. We next asked whether, in addition to the shared component, there also was an individually unique component to the representation. To test for an individually unique component, we compared the within-subject RDM replicability with the between-subject RDM replicability. This procedure enabled us to assess individual differences in the representation of particular objects while accounting for differences caused by day-to-day variations of the physiological and psychological state of the subject, the physical state of the scanner, and measurement noise. If the brain representations were individually unique, this uniqueness would manifest in a greater within- than between-subject RDM correlation. We calculated the difference in RDM replicability (average within-subject r minus average between-subject r) as an individuation index (i-index) that reflects the evidence for individual uniqueness of the representational geometry (Fig. 3*A*). To determine whether the i-index was significant, we used a subject-label randomization test (*SI Materials and Methods* and Fig. S6).

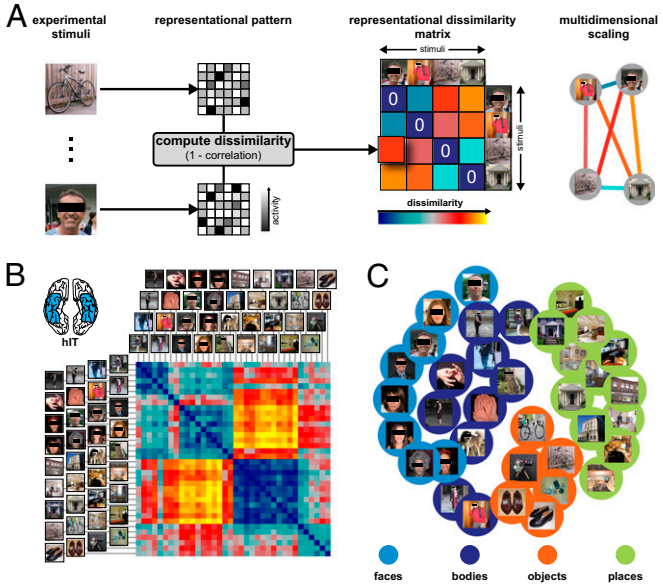

Fig. 2. Representational similarity analysis and human inferior temporal cortex representational geometry. (*A*) For each pair of stimuli, the response patterns in a brain region are compared to determine the stimuli's representational dissimilarity. The dissimilarity between two patterns is measured as 1 minus the Pearson correlation across voxels. These dissimilarities are assembled in the RDM, which is symmetric about a diagonal of zeros. (*B*) The mean hIT RDM for the 36 unfamiliar images, obtained by averaging hIT RDMs across subjects and scanning days. (*C*) Multidimensional scaling (metric stress) finds a 2D arrangement of the stimuli in which the distance between each pair reflects the dissimilarity of their activity patterns.

For unfamiliar objects, EVC [*i*-index = 0.09, *P*(average within-subject *r* > average between-subject *r*) < 0.0001] and hIT [*i*-index = 0.10, *P*(average within-subject *r* > average between-subject *r*) < 0.0001] both exhibited individually unique representational geometries. For personally meaningful objects, the *i*-index was not significant in EVC [*i*-index = 0.03, *P*(average within-subject *r* > average between-subject *r*) > 0.05], but it was significant in hIT [*i*-index = 0.1, *P*(average within-subject *r* > average between-subject *r*) < 0.005] (Fig. 4*A*). For further within- and between-category analyses, methodological details, and effects of ROI sizes, see Figs. S5–S7.

The *i*-index depends on the number of stimuli, the amount of noise, and the amount of data averaged. To obtain a more generalizable estimate of the strength of the individually unique component, we estimated the individually unique pattern variance as a proportion of the nonnoise pattern variance (*SI Materials and Methods*). For hIT, the individually unique pattern component accounts for about 12.5% of the nonnoise pattern variance.

In sum, we found replicable and individually unique representational geometries for both unfamiliar and familiar objects in hIT and, to a lesser degree, in EVC. The individually unique component was evident alongside the previously described categorical divisions shared among subjects. Our findings thus suggest that representational geometries in different individual brains are, like siblings, at once similar and significantly distinct. If these individually unique response-pattern geometries constitute the neural substrate of each individual's unique perception of the objects, they should be reflected in individual judgments of object similarity.

Similarity Judgments Reflect Each Individual's hIT Representation. To investigate the relationship between response-pattern geometries and behavior, we asked our subjects to perform similarity judgments. The judgments were acquired using a computer-based task, in which the subjects arranged the objects on a screen by mouse drag-and-drop operations so that the distance between any two objects reflected their perceived dissimilarity (*Materials and Methods* and Fig. 1*B*) (32, 33).

hIT and similarity judgments share basic categorical divisions in all subjects. As previously reported (30), the similarity judgments emphasized categorical divisions similar to those observed in the hIT response patterns, exhibiting categorical clusters corresponding to bodies, faces, places, and objects and a clear animate/inanimate division (Fig. S2*B*). As expected based on these categorical divisions evident in both hIT and judgments, RDMs were significantly correlated between hIT (RDMs averaged across scanning days) and judgments for both unfamiliar (average within-subject $r = 0.22$, $P < 0.0001$; average between-subject $r = 0.22$, $P < 0.0001$; stimulus-label randomization test) and familiar objects (average within-subject $r = 0.23$, $P < 0.0001$; average between-subject $r = 0.18$, $P < 0.0001$). In contrast, there was no evidence for a relationship between the representation in EVC and the similarity judgments for either unfamiliar (average within-subject r = −0.01, $P > 0.05$; average between-subject r = −0.02, $P > 0.05$) or familiar objects (average within-subject r = −0.02, $P > 0.05$; average between-subject $r = -0.04$, $P > 0.05$) (Fig. S3).

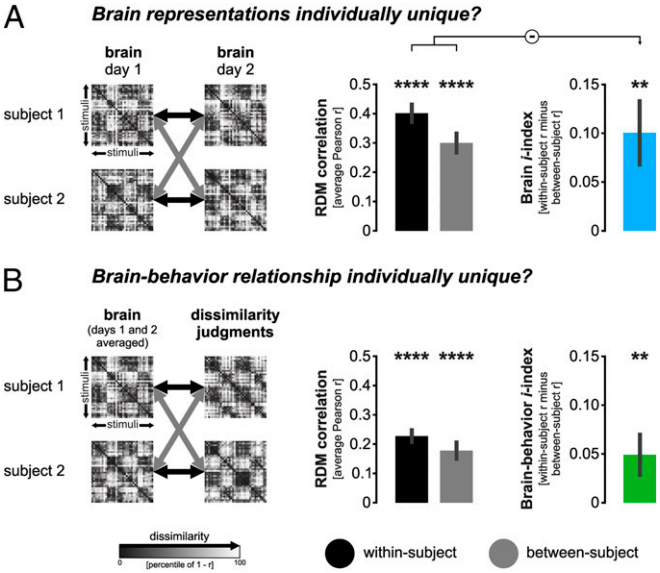

Fig. 3. Comparing dissimilarity matrices within and between individuals reveals individually unique brain representations and brain–behavior relationships. (*A*) For each subject and scanning day, we computed an RDM (Fig. 2) from the measured brain-activity patterns. We computed the RDM replicabilities (Pearson correlation between lower-triangular entries) across scanning days, within subjects (black double arrows), and between subjects (gray double arrows). Within-subjects (black bar) and between-subjects (gray bar) RDM replicabilities across scanning days were highly significant. For each pair of subjects, we computed an *i*-index (blue bar) as the average within-subject RDM replicability minus the average between-subject RDM replicability, averaged across subject pairs. Data shown are for the hIT representation of familiar images. The *i*-index was significant, indicating that different subjects have distinct representational geometries in hIT. (*B*) We used the same approach to test the brain–behavior relationship and its individual uniqueness, considering the correlations between brain RDMs (averaged across the two scanning days) and behavioral RDMs (reflecting the similarity judgments performed by each subject). The brain–behavior relationship was highly significant within and between subjects for hIT. The brain–behavior *i*-index was significant as well, indicating that idiosyncrasies of a subject's similarity judgments are predicted by that subject's hIT representational geometry. In *A* and *B*, results are for the 36 familiar images. Significance of the *i*-index (****$P < 0.0001$, ***$P < 0.001$, **$P < 0.01$, *$P < 0.05$, all Bonferroni-adjusted for two tests for regions EVC and hIT) was assessed by randomization of the subject labels. Error bars represent the SEM, estimated by bootstrap resampling of the set of subject pairs.

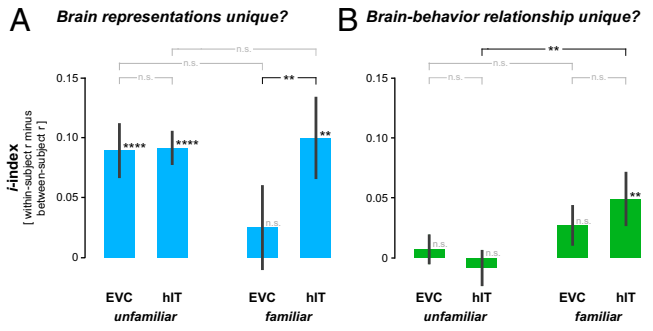

Fig. 4. hIT has an individually unique representational geometry that predicts individual judgment idiosyncrasies for familiar objects. (*A*) Brain *i*-indices indicating individually unique brain representations. The *i*-index (Fig. 3) was highly significant in EVC and hIT for unfamiliar objects. For familiar objects, the *i*-index was significant in hIT but not in EVC and was significantly larger in hIT than in EVC. (*B*) Brain–behavior *i*-indices, indicating that a subject's brain representation predicts idiosyncrasies of his or her similarity judgments, were significant only for hIT and only for familiar objects ($P < 0.005$, uncorrected; $P < 0.01$ adjusted for two tests in regions hIT and EVC). The brain–behavior *i*-index was significantly higher in hIT for familiar than for unfamiliar objects. ****$P < 0.0001$, **$P < 0.01$; n.s., not significant, Bonferroni-adjusted for two tests (for regions EVC and hIT). Interactions were tested by bootstrap resampling of the subject pairs.

hIT predicts individual judgment idiosyncrasies for familiar objects. If an individual's brain representation predicted that person's similarity judgments better than another person's, we would have evidence that the region in question has a role in representing the individually unique percept. We tested for a greater within- than between-subject brain-to-behavior RDM correlation using a subject-label randomization test (Fig. 3*B*). For the unfamiliar objects, the test revealed no evidence for a better prediction of the similarity judgments within than between subjects in EVC [*i*-index = –0.007, *P*(average within-subject *r* > average between-subject *r*) > 0.05] or in hIT [*i*-index = –0.008, *P*(average within-subject *r* > average between-subject *r*) > 0.05).

We next considered this relationship for familiar objects. The brain-to-behavior RDM correlation for the familiar objects was significantly larger within than between subjects in hIT [*i*-index = 0.05, *P*(average within-subject *r* > average between-subject *r*) < 0.01] but not in EVC [*i*-index = 0.02, *P*(average within-subject *r* > average between-subject *r*) > 0.05] (Fig. 4*B*). An individual's unique hIT representation thus predicts idiosyncrasies in that person's similarity judgments when the objects are personally meaningful.

An overview of all inferential results for EVC and hIT and also for V1, V2, LOC, FFA, and the PPA is given in Fig. 5.

Discussion

Previous studies have shown that the basic categorical divisions of IT are shared among people (20–22) and even among primate species (23). Here we demonstrated that beyond this shared categorical structure, the hIT representational geometry of particular bodies, faces, places, and man-made objects is individually unique. Moreover, the representation predicted each subject's own similarity judgments (more closely than other subjects') when the objects were personally meaningful. This result suggests that hIT forms part of the neural substrate of our individually unique perception of objects and their similarity relationships. In addition, our results demonstrate that subtle, individually unique representations of particular objects can be captured with fMRI.

Further analyses showed clear evidence that the within-category representational distances were individually unique in both EVC and hIT, whereas the evidence for individually unique between-category-centroid distances was weaker (*SI Results*, section 1).

We found evidence for an individually unique representation predictive of perceptual idiosyncrasies in hIT (but not in early visual areas) and for personally meaningful (but not for unfamiliar) objects. EVC also exhibited an individually unique representation but did not significantly predict perceptual idiosyncrasies. The object similarity judgments were likely based on higher-level visual and semantic representations. Such representations are hosted in hIT, and not in EVC. hIT might explain individual judgment idiosyncrasies here because the judgments were based on its representation. EVC might predict judgments of low-level visual similarity and their idiosyncrasies in individual subjects—a hypothesis to be tested in future studies. As a step in that direction, subjective percepts of visual size, a particular nonsemantic property, have been shown to be correlated with the early visual representation (36).

Functional differences as reported here ultimately must arise from differences in the physical structure of each individual brain. As a potential confound, functionally irrelevant anatomical idiosyncrasies, for example in the precise cortical folding pattern in a particular subject, probably have some effect on our estimates of representational geometry. Functionally irrelevant anatomical variation therefore might have inflated the *i*-indices. However, the idiosyncrasies of hIT representational geometries were predictive of idiosyncrasies in similarity judgments and thus were functionally relevant, ruling out the possibility that the representational idiosyncrasies we observed are driven entirely by functionally irrelevant anatomical variation.

What functionally relevant aspects of brain structure might explain the functional idiosyncrasies we observed? The microstructure of cortical circuits certainly is unique to each individual. However, even at the level of gross anatomy, substantial variation has been reported to predict behavioral measures. For example, the size of primary visual cortex varies across individuals by a factor of about 2.5 (37, 38). Interindividual variation in V1 cortical magnification predicts variation of the magnitude of visual size illusions across subjects (3, 39). Although other areas might vary by smaller factors, many parts of the brain, including cortical and subcortical structures, show gross anatomical variation across individuals that is predictive of cognitive and

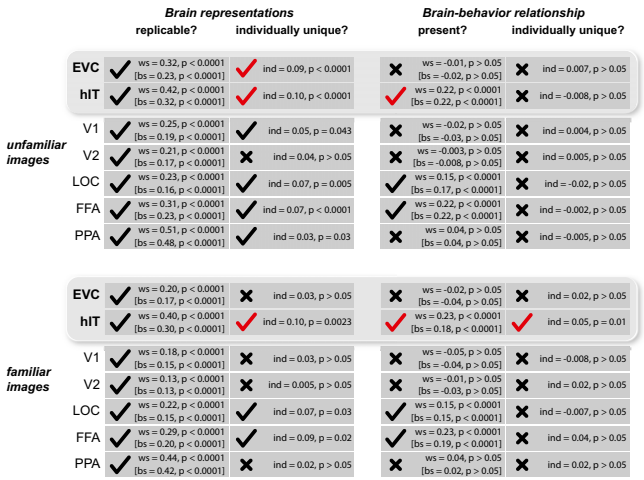

Fig. 5. Summary of results. Significant results are marked with a checkmark (in red for important novel results in regions EVC and hIT, for which we had specific prior hypotheses). For the replicability results, the checkmarks indicate significant within-subject replicability. Nonsignificant results are marked with an X. RDM correlations (Pearson correlation coefficients: bs, between-subject; ws, within-subject,), *i*-indices (ind = ws – bs), and the associated Bonferroni-adjusted *P* values are reported also. For summary ROIs EVC and hIT, for which we had prior hypotheses, Bonferroni adjustment was performed for two tests. For the other five ROIs, Bonferroni adjustment was performed for five tests.

behavioral differences (40). Our study demonstrates individual differences in high-level semantic representations but cannot address their structural basis. Our current interpretation is that the representational idiosyncrasies might arise from the microstructural plasticity of cortex, which is driven by individual experience.

At the level of function, a brain region's representation reflects feedforward stimulus processing and feedback from higher-level regions. Both feedforward and feedback processing could contribute to an individually unique representational geometry. For EVC, the known anatomical differences are likely to affect feedforward and lateral recurrent processing, providing one possible explanation for the individually unique early representation. In addition, the patterns of feedback elicited by each image might be individually unique. For example, an individual's interests might affect the spatial distribution of attention during the viewing of a given image. Individually unique patterns of attention-related response enhancements could contribute to the idiosyncrasies of the early visual representation. Even if such attentional patterns originate from high-level representations, there is no reason to expect two objects whose images elicit similar spatial distributions of attention to be judged as similar. An attentional account therefore also would be consistent with the failure of the early visual dissimilarities to predict the object similarity judgments.

Predictive coding theory provides another feedback-based interpretation of our early visual results. Predictive coding theory suggests that the activity in early visual cortex decreases when higher regions "explain away" aspects of the stimulus through feedback (41–43). This feedback would reduce overall activation for familiar images compared with unfamiliar images. Consistently, we observed significantly reduced activation in early visual areas for the familiar images as compared with the unfamiliar images (Fig. S8). We also observed significantly reduced activation for the unfamiliar objects in scanning day 2 as compared with day 1, suggesting a further familiarization effect. The top-down suppression of expected aspects of the representation also should lead to reduced replicability of an individual's RDM in EVC for familiar images. In fact, we observed lower RDM replicability in EVC for personally meaningful objects.

In hIT, as well, both feedforward and feedback processing might contribute to the individually unique representations. Our finding that judgment idiosyncrasies were significantly predictable from hIT only for the personally meaningful objects suggests a specific role for feedback from the memory-related regions of the medial temporal lobe (44). For example, inferred or associated scene components might be added to the representation in hIT through feedback. This mechanism appears possible because hIT can represent both perceived and remembered or imagined objects (45–47) and can simultaneously represent multiple objects (48, 49). In addition, the hIT representation is known to be plastic, reflecting an individual's experience (50).

Mnemonic enrichment might be expected to expand the representational distances among personally meaningful objects that have distinct associations. Alternatively, mnemonic enrichment might be expected to contract the representational distances between objects that have shared associations. We found no evidence for either an expansion or a contraction of hIT representational distances related to familiarity (*SI Results*, section 2). One interpretation of this negative finding is that mnemonic enrichment effects are weak or absent. Another possibility is that the effects of distinct and shared associations cancel out across all object pairs. Individually unique memory associations that affect both the hIT representation and the similarity judgments would be consistent with our finding that judgment idiosyncrasies reflected idiosyncrasies in the hIT representation.

It is important to note that the predictions of perceptual idiosyncrasies from the hIT representation, although robustly better than chance, are not very precise. Precision estimates (*SI Results*, section 3) depend on many factors, including the number of stimuli and the amount of averaging, and have little meaning beyond the context of a particular study and analysis. Predicting a complex representational geometry is fundamentally more challenging than predicting a unidimensional or binary variable. Our results provide an important proof of concept. In the future, individual measurements of representational geometries might contribute to certain clinical applications, especially as technology advances. For example, our approach might lend itself to characterizing how individual representations develop over the lifespan, how they differ between groups, and how they are affected in disorders. There is a broad range of clinical disorders that affect perception, including object agnosias (51), autism (52), and Alzheimer's disease (53). It might be possible to track longitudinal changes in representational geometry in individuals as disorders develop, enabling us to observe the progression of a disorder and its response to therapeutic interventions at the level of representational geometry.

In sum, we have shown that the hIT representation in an individual predicts idiosyncrasies of that person's subjective perceptual experience. Our findings suggest that fMRI combined with pattern-information analyses has the power to open up the unique mental worlds of individuals for empirical study at the level of the brain.

Materials and Methods

Participants. Twenty subjects (10 female; mean age, 22.3 ± 4.12 y) with normal or corrected-to-normal vision were recruited for the study. They provided informed consent as part of a protocol approved by the Cambridge Psychology Research Ethics Committee. Each subject was scanned twice (median time window between scanning days, 11.5 ± 9 d).

Stimuli. Subjects were presented with 72 pictures of bodies, faces, places, and man-made objects (Fig. 1*A* and Fig. S1). Each subject viewed 18 images from his or her own photo album, 18 images from another subject's photo album, and 36 images that were shown to all subjects. The categories were equally frequent in these three stimulus groups, and the photo-album images fell into predefined conceptual slots (the subject's own face, parent's face, relative's face, partner's face, friend's face, own hands, relative's body, friend's body, familiar pet, own bedroom, own living room, own kitchen, front of own house, own work place, own office desk/working environment, own keys, own shoes, own vehicle) (Fig. S1). The subjects were instructed to provide images with a minimal resolution of 600 × 600 pixels. All images were inspected visually before experimentation for sharpness and general quality. The 36 general objects were selected from a database of object images held in our laboratory. All images were cropped or scaled at a resolution of 600 × 600 pixels. All stimuli used in the experiments subtended ∼10° of visual angle.

Similarity Judgments: Multiple Arrangement Method. As part of the behavioral testing, the subjects performed a similarity judgments task. The multiple arrangement (MA) method allows subjects to communicate multiple object-pair similarities at once. In the MA method, subjects communicate perceived object similarity by arranging multiple object images in 2D on a computer screen by mouse drag-and-drop. Our MA method uses adaptive selection of object subsets during measurement to estimate efficiently the similarity perceived by each individual subject. The MA method has been described in detail, and its test–retest reliability (r = 0.81) and external validity were established in ref. 33. The subjects were instructed, "Please arrange these objects according to their similarity" so that similar objects were placed close together, and dissimilar objects were placed further apart. During the MA task, a partial RDM is obtained after each trial, and the multiple partial matrices are combined to give a single estimate of the entire similarity judgments RDM.

fMRI. Scanning was carried out at the Medical Research Council–Cognition and Brain Sciences Unit (Cambridge, UK) using a 3-Tesla Siemens Tim Trio MRI scanner with a 12-channel head coil. Functional data were acquired using T2*-weighted echoplanar images (64 × 64; 3 × 3 mm in-plane voxel size; slices 3.75 mm thick; TR: 2 s; TE: 30 ms; flip angle: 78°). The acquisition window was tilted up ∼30° from the horizontal plane to provide complete coverage of the occipital and temporal lobes. Volumes were collected in nine continuous runs for each participant. The initial eight volumes from the runs were discarded to allow for scanner equilibration effects. Additionally, magnetization-prepared rapid gradient echo structural images were acquired (256 × 240 × 192; 1 mm^3 isotropic voxels; TR: 2,250 ms; TE: 2.99 ms; flip angle: 9°).

Imaging Analysis. Preprocessing of the fMRI data was carried out using Statistical Parametric Mapping 8 (SPM8; www.fil.ion.ucl.ac.uk/spm/) and Matlab independently for each scanning day. All functional volumes were realigned to the first nondiscarded volume, slice time corrected, and coregistered to the T1 structural volume. The functional volumes remained unsmoothed and in their native space. For each voxel, we fit the time-series data using GLMdenoise version 1.1 (http://kendrickkay.net/GLMdenoise/). GLMdenoise implements a general linear model (GLM) analysis of fMRI data and uses noise regressors derived from task-unrelated voxels to improve the accuracy of beta weight estimates (54, 55). The GLM was modeled with a separate set of regressors for each object item (72 objects + one extra regressor for the anomaly detection trials). From this procedure, we obtained single-image blood oxygen-level–dependent fMRI activation estimates. Contrast images for each individual condition against the implicit baseline were generated based on the fitted responses. The resulting t contrast images were used as inputs for representational similarity analysis (16) in the EVC and hIT ROIs (Fig. S9). Note that statistical inference on the RDMs (*SI Materials and Methods*) does not rely on the estimates of the noise level over the fMRI time course but on the independent RDM estimates obtained for each scanning day and subject.

ACKNOWLEDGMENTS. We thank R. Berkers, M. Mur, B. Staresina, M. Anderson, and M. Wimber for comments on a draft of this paper, and K. Kay and R. N. Henson for advice on data analysis. This work was supported by UK Medical Research Council Grant MC-A060-5PR60 and by European Research Council Starting Grant ERC-2010-StG 261352 (to N.K.).

1. Hasson U, Nir Y, Levy I, Fuhrmann G, Malach R (2004) Intersubject synchronization of cortical activity during natural vision. *Science* 303(5664):1634–1640.
2. Ochsner KN, Bunge SA, Gross JJ, Gabrieli JDE (2002) Rethinking feelings: An FMRI study of the cognitive regulation of emotion. *J Cogn Neurosci* 14(8):1215–1229.
3. Schwarzkopf DS, Song C, Rees G (2011) The surface area of human V1 predicts the subjective experience of object size. *Nat Neurosci* 14(1):28–30.
4. Puce A, Allison T, Gore JC, McCarthy G (1995) Face-sensitive regions in human extrastriate cortex studied by functional MRI. *J Neurophysiol* 74(3):1192–1199.
5. Martin A, Wiggs CL, Ungerleider LG, Haxby JV (1996) Neural correlates of category-specific knowledge. *Nature* 379(6566):649–652.
6. Malach R, et al. (1995) Object-related activity revealed by functional magnetic resonance imaging in human occipital cortex. *Proc Natl Acad Sci USA* 92(18):8135–8139.
7. Kanwisher N, McDermott J, Chun MM (1997) The fusiform face area: A module in human extrastriate cortex specialized for face perception. *J Neurosci* 17(11):4302–4311.
8. Epstein R, Kanwisher N (1998) A cortical representation of the local visual environment. *Nature* 392(6676):598–601.
9. Grill-Spector K, Kushnir T, Edelman S, Itzchak Y, Malach R (1998) Cue-invariant activation in object-related areas of the human occipital lobe. *Neuron* 21(1):191–202.
10. Haxby JV, et al. (2001) Distributed and overlapping representations of faces and objects in ventral temporal cortex. *Science* 293(5539):2425–2430.
11. Kriegeskorte N, Formisano E, Sorger B, Goebel R (2007) Individual faces elicit distinct response patterns in human anterior temporal cortex. *Proc Natl Acad Sci USA* 104(51): 20600–20605.
12. Kay KN, Naselaris T, Prenger RJ, Gallant JL (2008) Identifying natural images from human brain activity. *Nature* 452(7185):352–355.
13. Mur M, et al. (2012) Categorical, yet graded—single-image activation profiles of human category-selective cortical regions. *J Neurosci* 32(25):8649–8662.
14. Huth AG, Nishimoto S, Vu AT, Gallant JL (2012) A continuous semantic space describes the representation of thousands of object and action categories across the human brain. *Neuron* 76(6):1210–1224.
15. Kiani R, Esteky H, Mirpour K, Tanaka K (2007) Object category structure in response patterns of neuronal population in monkey inferior temporal cortex. *J Neurophysiol* 97(6):4296–4309.
16. Kriegeskorte N, Mur M, Bandettini P (2008) Representational similarity analysis - connecting the branches of systems neuroscience. *Front Syst Neurosci* 2:4.
17. Naselaris T, Stansbury DE, Gallant JL (2012) Cortical representation of animate and inanimate objects in complex natural scenes. *J Physiol Paris* 106(5-6):239–249.
18. Polyn SM, Natu VS, Cohen JD, Norman KA (2005) Category-specific cortical activity precedes retrieval during memory search. *Science* 310(5756):1963–1966.
19. Xue G, et al. (2010) Greater neural pattern similarity across repetitions is associated with better memory. *Science* 330(6000):97–101.
20. Shinkareva SV, Malave VL, Just MA, Mitchell TM (2012) Exploring commonalities across participants in the neural representation of objects. *Hum Brain Mapp* 33(6): 1375–1383.
21. Raizada RDS, Connolly AC (2012) What makes different people's representations alike: Neural similarity space solves the problem of across-subject fMRI decoding. *J Cogn Neurosci* 24(4):868–877.
22. Haxby JV, et al. (2011) A common, high-dimensional model of the representational space in human ventral temporal cortex. *Neuron* 72(2):404–416.
23. Kriegeskorte N, et al. (2008) Matching categorical object representations in inferior temporal cortex of man and monkey. *Neuron* 60(6):1126–1141.
24. Norman KA, Polyn SM, Detre GJ, Haxby JV (2006) Beyond mind-reading: Multi-voxel pattern analysis of fMRI data. *Trends Cogn Sci* 10(9):424–430.
25. Haynes JD, Rees G (2006) Decoding mental states from brain activity in humans. *Nat Rev Neurosci* 7(7):523–534.
26. Weiner KS, Grill-Spector K (2010) Sparsely-distributed organization of face and limb activations in human ventral temporal cortex. *Neuroimage* 52(4):1559–1573.
27. Spiridon M, Kanwisher N (2002) How distributed is visual category information in human occipito-temporal cortex? An fMRI study. *Neuron* 35(6):1157–1165.
28. O'Toole AJ, Jiang F, Abdi H, Haxby JV (2005) Partially distributed representations of objects and faces in ventral temporal cortex. *J Cogn Neurosci* 17(4):580–590.
29. Harel A, Kravitz DJ, Baker CI (2013) Deconstructing visual scenes in cortex: Gradients of object and spatial layout information. *Cereb Cortex* 23(4):947–957.
30. Mur M, et al. (2013) Human Object-Similarity Judgments Reflect and Transcend the Primate-IT Object Representation. *Front Psychol* 4:128.
31. Suzuki WA, Amaral DG (1994) Perirhinal and parahippocampal cortices of the macaque monkey: Cortical afferents. *J Comp Neurol* 350(4):497–533.
32. Goldstone R (1994) An efficient method for obtaining similarity data. *Behav Res Methods Instrum Comput* 26(4):381–386.
33. Kriegeskorte N, Mur M (2012) Inverse MDS: Inferring dissimilarity structure from multiple item arrangements. *Front Psychol* 3:245.
34. Aguirre GK (2007) Continuous carry-over designs for fMRI. *Neuroimage* 35(4):1480–1494.
35. Kriegeskorte N, Kievit RA (2013) Representational geometry: Integrating cognition, computation, and the brain. *Trends Cogn Sci* 17(8):401–412.
36. Murray SO, Boyaci H, Kersten D (2006) The representation of perceived angular size in human primary visual cortex. *Nat Neurosci* 9(3):429–434.
37. Dougherty RF, et al. (2003) Visual field representations and locations of visual areas V1/2/3 in human visual cortex. *J Vis* 3(10):586–598.
38. Stensaas SS, Eddington DK, Dobelle WH (1974) The topography and variability of the primary visual cortex in man. *J Neurosurg* 40(6):747–755.
39. Schwarzkopf DS, Rees G (2013) Subjective size perception depends on central visual cortical magnification in human v1. *PLoS ONE* 8(3):e60550.
40. Kanai R, Rees G (2011) The structural basis of inter-individual differences in human behaviour and cognition. *Nat Rev Neurosci* 12(4):231–242.
41. Mumford D (1992) On the computational architecture of the neocortex. II. The role of cortico-cortical loops. *Biol Cybern* 66(3):241–251.
42. Rao RPN, Ballard D (1999) Predictive coding in the visual cortex: A functional interpretation of some extra-classical receptive-field effects. *Nature Neuroscience* 2(1): 79–87.
43. Murray SO, Kersten D, Olshausen BA, Schrater P, Woods DL (2002) Shape perception reduces activity in human primary visual cortex. *Proc Natl Acad Sci USA* 99(23): 15164–15169.
44. Staresina BP, Henson RNA, Kriegeskorte N, Alink A (2012) Episodic reinstatement in the medial temporal lobe. *J Neurosci* 32(50):18150–18156.
45. Lee S-H, Kravitz DJ, Baker CI (2012) Disentangling visual imagery and perception of real-world objects. *Neuroimage* 59(4):4064–4073.
46. Stokes M, Thompson R, Cusack R, Duncan J (2009) Top-down activation of shape-specific population codes in visual cortex during mental imagery. *J Neurosci* 29(5): 1565–1572.
47. Cichy RM, Heinzle J, Haynes J-D (2012) Imagery and perception share cortical representations of content and location. *Cereb Cortex* 22(2):372–380.
48. Reddy L, Kanwisher NG, VanRullen R (2009) Attention and biased competition in multi-voxel object representations. *Proc Natl Acad Sci USA* 106(50):21447–21452.
49. Macevoy SP, Epstein RA (2009) Decoding the representation of multiple simultaneous objects in human occipitotemporal cortex. *Curr Biol* 19(11):943–947.
50. Op de Beeck HP, Baker CI, DiCarlo JJ, Kanwisher NG (2006) Discrimination training alters object representations in human extrastriate cortex. *J Neurosci* 26(50):13025–13036.
51. James TW, Culham J, Humphrey GK, Milner AD, Goodale MA (2003) Ventral occipital lesions impair object recognition but not object-directed grasping: An fMRI study. *Brain* 126(Pt 11):2463–2475.
52. Dakin S, Frith U (2005) Vagaries of visual perception in autism. *Neuron* 48(3):497–507.
53. Hoffman P, Jones RW, Ralph MAL (2012) The degraded concept representation system in semantic dementia: Damage to pan-modal hub, then visual spoke. *Brain* 135(Pt 12):3770–3780.
54. Kay KN, Winawer J, Mezer A, Wandell BA (2013) Compressive spatial summation in human visual cortex. *J Neurophysiol* 110(2):481–494.
55. Kay K, Rokem A, Winaver J, Dougherty R, Wandell B (2013) GLMdenoise: A fast, automated technique for denoising task-based fMRI data. *Front Neurosci* 7:247.